UVSOR

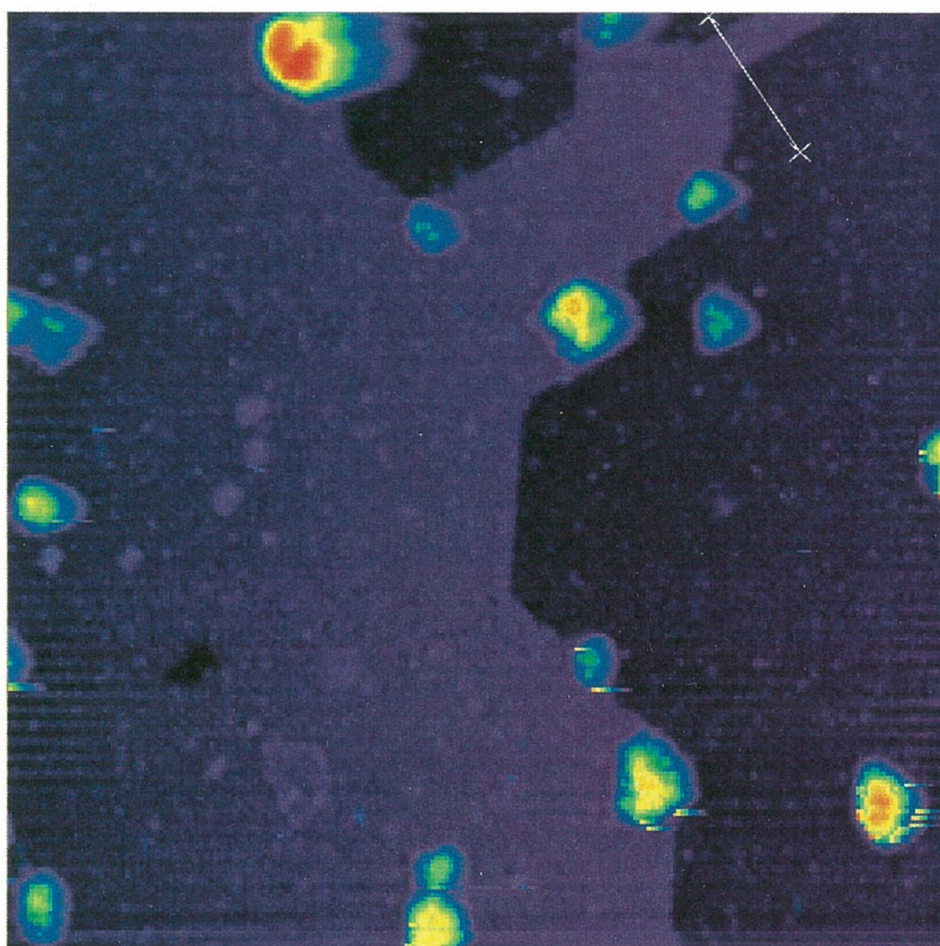

Surface & Photochemistry

BL2B1, 3A1, 4A1, 4B, 5A, 5B, 6A2, 8A

[BL5A]

Electronic states of organic molecule/Si surface hybrid systems

Jun Yoshinobu, Yoshiyuki Yamashita, Kozo Mukai, Kanae Hamaguchi, Shin-ichi Machida, Masashi Nagao and Fumiko Yasui

The Institute for Solid State Physics, University of Tokyo
7-22-1 Roppongi, Minato-ku, Tokyo 106-8666, Japan
(e-mail: yoshinobu@issp.u-tokyo.ac.jp)

In order to explore the candidate systems for nano-scale molecular device and chemical sensor, bonding and structures of several unsaturated hydrocarbons (ethylene, cyclopentene, cyclohexene, and 1,4-cyclohexadiene) chemisorbed on Si(100) have been investigated by means of photoelectron spectroscopy (PES) for both valence region and core level, scanning tunneling microscopy (STM) and high-resolution electron energy loss spectroscopy (HREELS).

Here we report some experimental results about adsorbed molecular systems using UVSOR-BL5A. Experiments have been performed in the UHV chamber including the apparatus for low energy electron diffraction (LEED), Auger electron spectroscopy (AES), photoelectron spectroscopy (PES) and gas dosing. The Si sample used was a Si(100) 5° vicinal surface. The clean one-domain Si(100)(2x1) surface was prepared by several flashing cycles up to ~1250℃ and annealing at ~600℃. The PES spectra of Si 2p and valence region were measured for the clean Si(100), saturated chemisorption layer and multilayer surfaces.

Ethylene on Si(100)(2x1) is a well established system which is di-σ bonded to the Si dimer [1]. The formation of this di-σ bond is due to the interaction between the π orbital of ethylene and the Si dangling bond. Adsorbed ethylene is stable up to 550-600K [1,2]. Thus, using such surface reaction including the di-σ bond formation, atomically controlled interface could be fabricated between an unsaturated hydrocarbon molecule and the Si(100) surface.

Hamers et. al. have reported that adsorbed cyclopentene molecules are well ordered on Si(100(2x1) and the molecule stands up on the surface by the use of STM and multiple internal reflection infrared absorption spectroscopy [3]. The present PES results have clearly indicated that the π orbital of cyclopentene and the Si dangling bond are interacted. Both PES and HREELS results indicate a single adsorption state. The electronic structure of the adsorbed cyclopentene is quite similar to cyclopentane.

In the case of cyclohexene adsorbed on Si(100), the situation is different. The PES spectra in valence and Si 2p regions are somewhat complex. Our STM observation shows that there are two adsorption states at least. According to the HREELS measurements, cyclohexene adsorbs molecularly. Two adsorbed states may originate from two different conformational isomers ("boat" and "chair" conformations) on the surface.

1,4-cyclohexadiene takes a single adsorption state on Si(100) according to the STM, HREELS and valence PES results. Valence PES shows that only one of two π orbitals of the molecule reacts with the Si dangling bond. Here an upright (standing-up) structure is proposed for the adsorbed molecule; the remaining π orbital protrudes towards the vacuum. Thus, this system may be a good candidate system for successive chemical reaction to fabricate more complex structure on the surface [4].

References

[1] J. Yoshinobu et.al., J. Chem. Phys. 87(1987)7332.
[2] L.Clemen et. al., Surf. Sci. 268(1992)205.
[3] R. J. Hamers et. al., J. Phys. Chem. 101(1997)1489.
[4] J. T. Yates, Jr., Science 229(1998)335.

(BL2B1)

Cs Adsorption on ZrC(111)

Kenichi OZAWA, Takashi YOSHII, Tetsu NODA, Kazuyuki EDAMOTO, Shinichiro TANAKA[1], Shigeki OTANI[2]

Department of Chemistry and Materials Science, Tokyo Institute of Technology, Meguro-ku, Tokyo 152-0033, Japan

[1] *Institute for Molecular Science, Okazaki-shi, Aichi 444-8585, Japan*

[2] *National Institute for Research in Inorganic Materials, Tsukuba-shi, Ibaraki 305-0044, Japan*

Room-temperature adsorption of Cs on the ZrC(111) surface has been studied by core-level photoemission spectroscopy. The work function of the substrate surface decreases monotonically upon Cs adsorption and approaches to the Cs metal value without showing a clear work function minimum. The Cs 4*d* core-level lineshape analysis indicates that the plasmon loss peak appears already in the very initial stages of adsorption. These results suggest that the adsorbed Cs atoms are in a metallic state by forming Cs islands and that adsorption proceeds via a growth of these islands.

1 Introduction

Alkali-metal adsorption has been attracted much attention because they are utilized for promoting a variety of surface chemical reactions, improving the electron emission from cathods, etc. Transition metal carbides (TMCs) are known to be a potential material for stable field electron emitters and catalysts which can be used in the extreme condition. Thus, adsorption of alkali metals on TMC surfaces are of great interest from the technological point of view.

Recently, we have investigated alkali-metal adsorption adsorption on the group IV and V TMC surfaces and found that the adsorption process is different depending on the low-index surfaces, i.e. (100) and (111) [1]. On the (100) surfaces, alkali metal adatoms tend to condence to form islands from the relatively low coverages. However, an ion-to-metal transition characterizes the adsorption process of alkali metals on the (111) surface. In the present study, we have investigated the adsorption process of Cs on ZrC(111) utilizing core-level PES in order further to elucidate the atom adsorption process on the TMC surface.

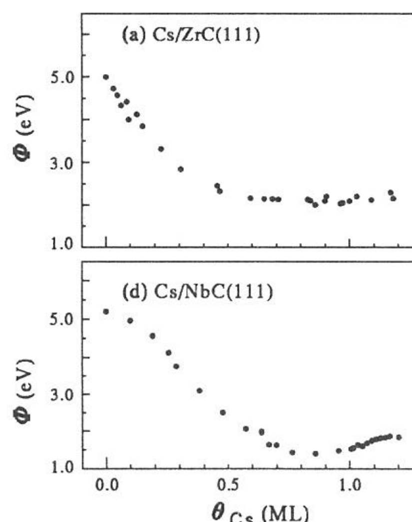

Fig. 1. (a) The work function change of ZrC(111) as a function of θ_{Cs}. (b) The work function change of NbC(111) as a function of θ_{Cs}.

2 Experimental

The core-level PES measurements utilizing synchrotron radiation were carried out at Beam Line 2B1, where the light was dispersed by a grasshopper monochromater. The photoelectron energy was analyzed by a double-pass cylindrical mirror analyzer. The ultrahigh vacuum (UHV) chamber was also equipped with an low energy electron diffraction (LEED) optics for the surface structural analysis and a mass spectrometer for the check of residual gases. The base pressure in the UHV system was less than 1.5×10^{-8} Pa.

A single crystal of $ZrC_{0.9}$ was grown by the floating-zone method at the National Institute for Research in Inorganic Materials. The (111) surface was cleaned by flashing to ~ 1800 K in the UHV chamber with electron bombardment from the rear of the sample disk. The Cs atoms were deposited on the surface at room temperature using a thoroughly outgassed commercial SAES dispenser.

3 Results and Discussion

Fig. 1a shows the Cs coverage (θ_{Cs}) dependence of the work function Φ of the ZrC(111) surface. As the surface is covered with Cs, Φ first decreases and approaches to 2 – 2.2 eV at $\theta_{Cs} > 0.6$ monolayer (ML). The total decrease is $\sim$ 3 eV. For comparison, the change in Φ for the Cs/NbC(111) system is shown in Fig. 1b. A similar behavior is seen in the Φ curve, i.e. a sharp decrease up to 0.8 ML. However, in contrast to the Cs/ZrC(111) system, further Cs adsorption on NbC(111) leads to a slight increase of $\sim$ 0.5 eV in Φ, forming a clear work function minimum. Φ approaches to $\sim$ 2 eV after the minimum for Cs/NbC(111) as in the case of Cs/ZrC(111). Considering that the work function of Cs metal is 2.14 eV [2], the property of the Cs overlayers at high coverages on both ZrC(111) and NbC(111) should be similar to that of Cs metal.

The metallization of the Cs overlayer at high θ_{Cs} is also proved from the Cs 4d core-level photoemission peak. The lower spectrum of Fig. 2a is the Cs 4d core-level spectrum for the 0.83 ML Cs-covered surface. The lineshape analysis reveals that the observed peak is composed of at least three components; one forms a main line and the other two components contribute to the tail structure to the high binding energy side of the main line. The latter two components are quenched by oxygen adsorption (upper spectrum of Fig. 2a). Moreover, the separation energies of these peaks from the main line are 1.9 and 4.7 eV, which are in good agreement with the energies of single and double losses of the Cs overlayer plasmon. Thus, the Cs overlayer at 0.83 ML has a metallic nature.

However, a similar tail structure is already observed at the Cs coverages of as low as 0.02 ML (Fig. 2b). A second component, shown as a shaded peak, is observed at the higher binding energy side of the main line by 1.9 eV. This is in good agreement of the plasmon energy, and thus the second component is attributed to the plasmon loss peak. In order to form a metallic overlayer in such a low coverage region, the Cs adatoms should condense to give a direct Cs–Cs interaction, which is requisite to form a Cs 6s metallic band. The work function change for this system also supports island formation from the low coverages. Fig. 1a shows that Φ decreases monotonically and approaches to the Cs metal value. This is in contrast to the work function change for Cs/NbC(111); the work function curve has a clear minimum at $\theta_{Cs} \simeq 0.8$ (Fig. 1b). Our recent study for the Cs/NbC(111) system has shown that, while the adsorbed Cs layer is metallic at high coverages, the Cs adatoms are partially ionized in the initial stages of adsorption [1]. Fig. 2c shows a lineshape

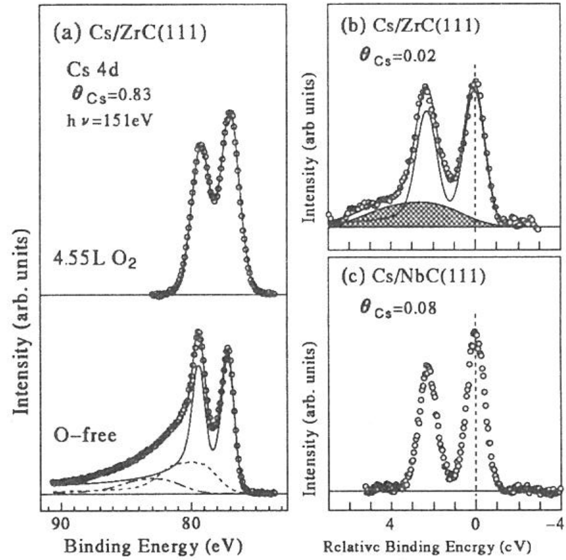

Fig. 2. Background-subtracted Cs 4*d* core-level spectra. Open circles are the observed data and the solid lines are the result of the lineshape analysis: (a) The Cs 4*d* spectra for the Cs-covered ZrC(111) surface (θ_{Cs} = 0.83 ML) and for the 0.83 ML Cs-covered surface which is exposed to 4.55 L oxygen. (b) The Cs 4*d* spectrum for Cs/ZrC(111) at θ_{Cs} = 0.02 ML. (c) The Cs 4*d* spectrum for Cs/NbC(111) at θ_{Cs} = 0.08 ML.

of the Cs 4*d* peaks at θ_{Cs} = 0.08, where adsorbed Cs is in an ionic state. Here, no tail structure associated with the plasmon loss is observed and the peaks are composed of two symmetric lines. This clearly demonstrates that the Cs adatoms are not in a metallic phase at low coverages. It is known that a depolarization process and the successive metallization of the alkali-metal overlayer lead to a minimum in the work function curve. Thus, the absence of the work function minimum for Cs/ZrC(111) implies that Cs adsorption proceeds without the formation of the surface dipole moment at low θ_{Cs} and its depolarization with increasing θ_{Cs}. The gradual approach of the work function to the value of Cs metal is, then, simply explained by a growth of the region covered with the Cs islands.

References

[1] K. Ozawa, S. Ishikawa, K. Edamoto, H. Kato and S. Otani: Surf. Sci. **419** (1999) 226, and references cited therein.

[2] H.B. Michaelson: J. Appl. Phys. **48** (1977) 4729.

(BL2B1)

Ion desorption from $TiO_2(110)$ surface

Shin-ichiro Tanaka[A], Kazuhiko Mase[B], Mitsuru Nagasono[C], Shin-ichi Nagaoka[D] and Masao Kamada[D]

[A]*Department of Physics, Graduate School of Science, Nagoya University, Nagoya 464-8602, Japan*
[B]*Institute of Material Structure Science, 305-0801, Tsukuba, Japan*
[C]*MAX-lab, Lund University, Box 118, S-221 00 Lund, Sweden*
[D]*Institute for Molecular Science, Myodaiji, Okazaki, 444-8585, Japan*

Desorption induced by electronic transition (DIET) from solid surfaces has been extensively studied in these decades. A general mechanism of ion desorption induced by core-level excitation has been proposed by Knotek and Feibelman, and been widely accepted as a standard mechanism. In the KF mechanism, a Ti3p core hole is produced by a primary excitation, and decays via an inter-atomic Auger process, because there are no higher-lying occupied electronic states at the Ti site (i.e., "maximal valency"), and thus an intra-atomic Auger decay is prohibited. If two Auger electrons and an additional electron are emitted from the oxygen atom, the remaining O^+ ion desorbs as a result of the Coulomb repulsion from the surrounding Ti^{4+} ions. However, results which contradict the KF model have been observed in several materials, e.g., Ti_2O_3, Na_xWO_3, Cr_2O_3. In these materials, O^+ desorption has been observed although the "maximal valency" criterion is not satisfied. Furthermore, an electronic configuration of $(Ti3d)^0(O2p)^6$ which has been assumed in the KF mechanism is not true. Recent theoretical studies have shown that the electronic states of the TiO_2 can not be explained with a single configuration, but instead a mixture of $Ti3d^n\underline{L}^{10-n}$ configurations is present. Here $\underline{L}$ and n stand for a hole in the oxygen (ligand) 2p orbital, and a nominal number of transferred charge from O2p to Ti3d through the hybridization between them, respectively. Thus, the "maximal valency" condition is not satisfied in TiO_2.

The electron–ion coincidence spectroscopy has been recently developed, and proved to be a very powerful tool for investigating the dynamics of the ion desorption induced by the core-level excitation and decay process. In the present report, the ion desorption induced by the core-level excitation is investigated by using the synchrotron radiation and the electron-ion coincidence technique. All the experiments were carried out at the BL-2B1. The $TiO_2(110)$ surface was cleaned by a number of cycles of Ar^+ ion sputtering and annealing. For removing the vacancy of oxygen at the surface, the sample was heated in the 10^{-6} Torr of oxygen once in three hours.

Figure 1 shows the photoelectron spectrum in the region of the O1s- and Ti2p-related Auger electrons (left part) and a series of electron-ion coincidence spectra (right part) of the photoelectron indicated by bars in the left part. The photon energy was 560 eV. Normalization were carried out using the total amount of signals mostly consisting of backgrounds, which were proportional to the photoelectron intensities. In fig.1, the peaks observed at about 1100 nsec are ascribed to the desorption of O^+. By assuming that the photoelectron intensity is proportional to the population of the final state of the Auger decay, the intensity of O^+ peak in the coincidence spectrum correlates to the desorption efficiency which is a function of the final state of the Auger decay. Peak area intensities derived from the summations of counts in the O^+ peaks (1048-1200 nsec) from the backgrounds and their errors derived from the standard deviation of the backgrounds are shown in figure 2 together with the photoelectron spectra.

At first, we discuss the ion desorption induced by the O1s core decay. Figure 2 indicates that O^+ yields does not correspond to the O-KVV Auger electrons. This can be related to the fact that oxygen in TiO_2 is nominally O^{2-}, therefore three electrons have to be removed from the oxygen atoms for the desorption of O^+. The final state of the normal Auger decay has only two holes at the valence band, and an additional process is necessary to produce O^+. The O^+ coincidence yield observed in the right panel of fig. 2 does not correspond to the normal Auger electron emission $[(O1s)^1(O2p)^6 \rightarrow (O1s)^2(O2p)^4]$ but to the shake-up Auger decay of O1s $[(O1s)^1(O2p)^6 \rightarrow (O1s)^2(O2p)^3(O3s)^1]$, which is minor process and can not be observed in the photoelectron spectrum. This is consistent with the recent photoelectron-photoion coincidence spectroscopy results, where the O^+ coincidence peak of the O1s shake-up satellite of O2p→O3s transition was larger than that of the O1s main peak. In this case, the shake-up excitation during the excitation and the following normal Auger decay $[(O1s)^1(O2p)^5(O3s)^1 \rightarrow (O1s)^2(O2p)^3(O3s)^1]$ produces three holes as a final state. This is a sort of an expansion of the KF mechanism although it is an intra-atomic process.

The desorption process induced by the Ti2p excitation, on the other hand, seems to be very different. In the photoelectron spectra, the Ti-$LM_{2,3}V$ and Ti-LVV electrons are observed (fig. 2). If the electronic configuration in the valence band of TiO_2 were assumed to be $(O2p)^6$ as in the KF model, this transition would be inter-atomic Auger transition. However, the O^+ desorption yield (normalized for the photoelectron intensity) does not result in a peak at the position of the (nominal) inter-atomic Auger transition or the shake-up transition. Instead, the O^+ desorption yield increases when a Ti3p hole is created as a final state of the Ti2p-initiated Auger decay. In fact, the Ti-LMV and Ti-LVV Auger transitions are not inter-atomic decay, but intra-atomic decay

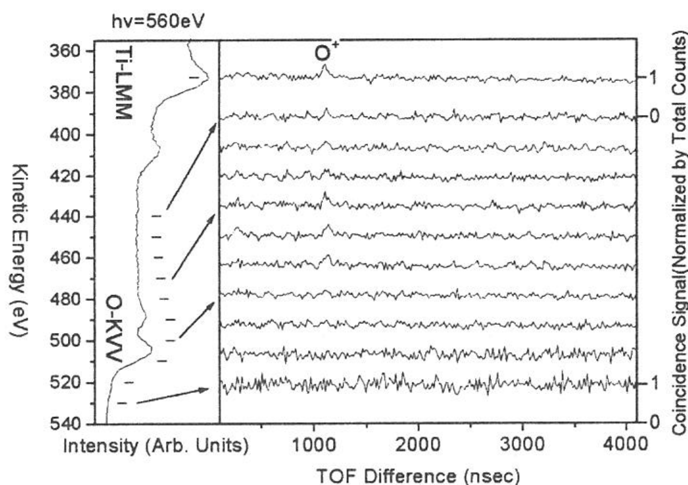

Figure 1

within the Ti site, because the charge transfer from O2p to Ti3d orbitals through their hybridization provides the Ti3d electron. Thus, the application of the KF model, in which the Ti3p:O2p:O2p inter-atomic Auger takes place because the Ti3p:Ti3d:Ti3d intra-atomic Auger decay is prohibited ("maximal valency"), is questionable.

Thus, another mechanism should be considered as the driving force for the creation of the O^+ and its desorption from $TiO_2(110)$ surface. According to the systematic study of the 3d transition metal oxides, a cluster model calculation based on the impurity Anderson model could successfully simulate the core photoelectron spectra using only a limited set of parameters. In the final state of the core level photoemission of 3d transition metal oxide, the core hole potential (U_{dc}) at the metal site pulls down the energy of the 3d levels, enabling a charge transfer from the O2p to metal to screen the core hole. A charge transfer from O2p to Ti3d through their hybridization (V_{eff}) is therefore a good candidate for the driving force of the O^+ desorption from $TiO_2(110)$ surface. It is likely to expect that a Ti3p core hole created by the Auger decay of Ti2p (and other core levels) can cause the charge transfer. This charge transfer may provide not only the change of the oxygen charge but also the re-arrangement of the valence electrons, which can add a repulsive potential due to an anti-bonding character of the new electronic states of the valence band. We would like to stress that this kind of re-arrangement of electronic configurations due to the core-hole potential is a multi-electron effect in solids. Therefore, a simple explanation such as that the main line corresponds to the single electron excitation and the satellite line corresponds to the two electron excitation in the photoelectron spectrum, which was valid in the O1s excitation, is not applicable to the excitation and decay of the Ti core level. Instead, the final state of the main line as well as the satellite line of Ti-related photoexcitation is due to a mixture of several electronic configurations, thus no shift was observed in fig. 2, and no enhancement of the O^+ yield was observed at the satellite line compared to the one at the main line of Ti-core levels in the photoelectron-photoion coincidence spectra.

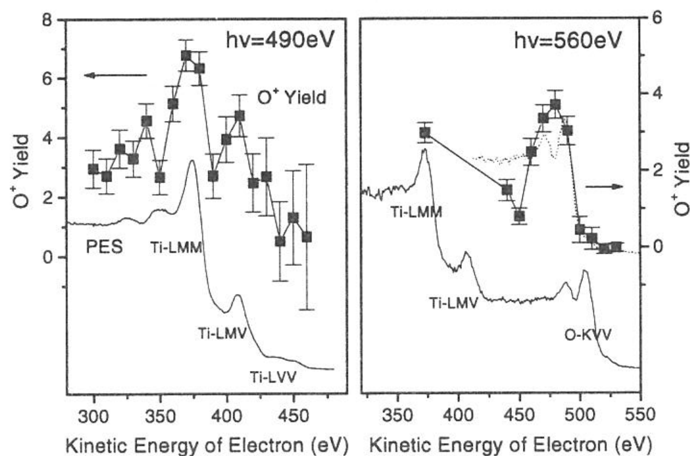

Figure 2

The new model can explain many of the results in the ion desorption from solid surfaces. This mechanism can be applied to early transition-metal compounds whose V_{eff} (mainly determined by number of the vacancy at the d orbital) is large. Thus, our model can explain the O^+ desorption not only from TiO_2, WO_3 and V_2O_5, but also from Ti_2O_3, Na_xWO_3 and Cr_2O_3, which could not be explained by the KF model. In late transition-metal compounds, V_{eff} is smaller, and thus the ion desorption is not expected, which is consistent with the experimental results. This model can also be applied to the early f-electron metal compounds like La_2O_3 and Er_2O_3 because the charge-transfer from O2p to metal f orbitals can be treated in a similar way as the one from O2p to metal d orbitals. In non-transition metal compounds, the mechanism can not be applied and it is expected that an excitation at the metal site does not yield the ion desorption. No ion desorption actually could observed in MgO and CaF_2 as a result of the Mg1s and Ca2p excitation. Thus, our model is more appropriate as a mechanism of the ion desorption from solid surfaces than the KF model.

(BL2B1)

O1s Core level shift on the Amorphous Ice Surface

Shin-ichiro Tanaka[A], Kazuhiko Mase[B], Mitsuru Nagasono[C], Shin-ichi Nagaoka[D] and Masao Kamada[D]

[A]Department of Physics, Graduate School of Science, Nagoya University, Nagoya 464-8602, Japan
[B]Institute of Material Structure Science, 305-0801, Tsukuba, Japan
[C]MAX-lab, Lund University, Box 118, S-221 00 Lund, Sweden
[D]Institute for Molecular Science, Myodaiji, Okazaki, 444-8585, Japan

Core-level photoelectron spectroscopy, also referred as XPS (X-ray photoelectron spectroscopy), has been used to investigate solids and solid surfaces. It is surface sensitive due to the small escape depth of the photoelectrons. The electron-ion coincidence (EICO) spectroscopy has been developed and used in order to investigate the mechanism of the ion desorption stimulated by the core excitation and to investigate the cite specific photochemistry in several systems. In EICO, only a photoelectron to correlate an ion desorption, i.e., a photoelectron ejected from the atoms from which ions desorb, can be detected. Considering the shorter escape depth of the ions than the electrons, the EICO spectroscopy is expected to give an information of electronic properties which is much more sensitive to the surface compared to the ordinal XPS. Thus, the EICO spectroscopy may be applicable not only to the investigation of the ion desorption from solid surfaces but also as a new tool for surface analysis.

In the present study, the EICO technique is applied to the ice surface for detecting the surface core level shift of the O1s level. Since the nature of the ice surface is of critical importance in many fields, extensive studies has been carried out. Although the photoelectron spectroscopy of the ice has been studied, there have been no study that reported the core level shift of O1s level on the ice surface to our knowledge. Ion desorption stimulated by the electron transition from the ice surface has been investigated theoretically, by the electron impact and by the photons of the O1s excitation region. According to these studies, the H^+ desorption after the O1s excitation is induced by the two hole final states of the Auger decay.

The experiments were carried out in a UHV chamber located at BL2B1 with a grasshopper monochromator (grating: 1800/mm). The chamber was equipped with a home-made EICO apparatus consisting of a cylindrical mirror analyzer (CMA) for electrons and a time-of-flight (TOF) mass analyzer for ions. Amorphous ice film was produced on the $TiO_2(110)$ surface exposed to gaseous water at 100K. Water was dosed via a stainless steal tube located in front of the sample with a pulsed valve. Film thickness of the ice was thick enough to exclude the affect of the substrate on the ion desorption and thin enough to avoid the charging effect. Measurements were carried out at 100K.

The figure below shows a series of photoelectron-photoion coincidence (PEPICO) spectra of amorphous ice taken at hv=680eV in the region of the O1s phototelectron in 0.5 eV steps. The desorption of H^+ in coincidence with the O1s photoelectrons are observed at around 250 ns, the intensity of which shows a maximum near the kinetic energy of 139 eV. Any other species like O^+ and OH^+ were not observed due to

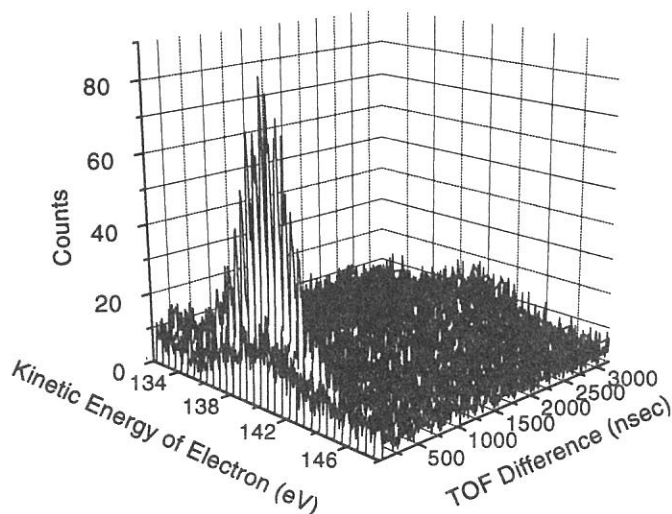

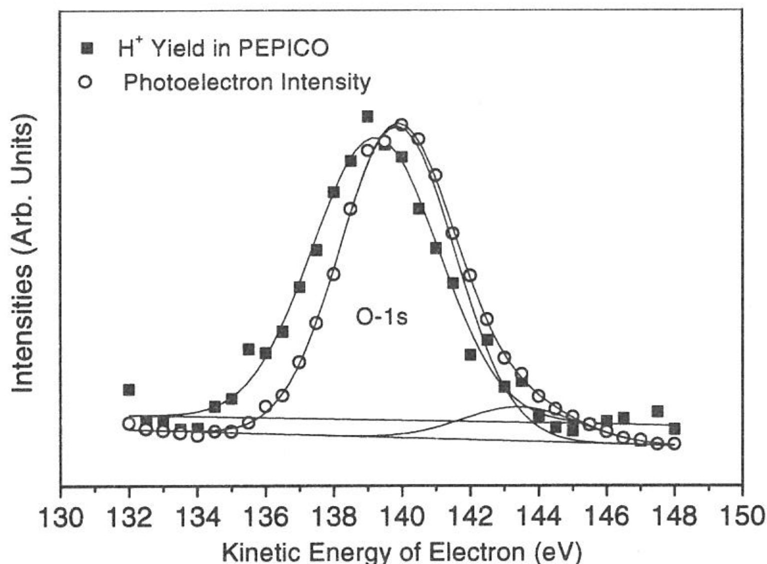

smaller desorption efficiencies. The desorption of H^+ is due to the repulsive final states as a result of the decay of the O1s hole. The energy of photons was far beyond the O1s threshold, and thus the effect of the excitation to the specific boundary state, e.g., $4a_1$ antibonding state, can be eliminated. The peak of the H^+ PEPICO yield spectrum, however, did not precisely agree with the peak in the photoelectron spectrum. In the figure above, area intensities of H^+ peak (200-320 nsec) in the PEPICO spectra (solid square) are plotted together with photoelectron intensities obtained simultaneously (open circle) as a function of the kinetic energy of photoelectrons. Lines are Gaussian curves with linear backgrounds as a result of the least square fitting calculation. A small component at ~144 eV in the photoelectron spectrum is due to the O1s emission from the TiO_2 substrate. Obviously, the H^+ yield is not in agreement with the photoelectron intensity. In fact, the peak position of the H^+ desorption yield is shifted to lower kinetic energy by about 0.7 eV compared to the photoelectron peak. This shift can be interpreted to the difference in the binding energy of the O1s level of H_2O from which the hydrogen atoms desorbs. According to the previous study, ice surface has several types of H_2O molecules, which are two- or three-coordinated molecules with a dangling hydrogen, two- or tree-coordinated molecules with a dangling oxygen coordination, and four-coordinated molecules with distorted tetrahedra. It seems to be likely to assume that the hydrogen ions desorbes from the molecule with a dangling hydrogen (probably with two coordination) due to the weaker bond between the hydrogen atom and the surface. Thus, the PEPICO spectroscopy only reflects the binding energy of oxygen atoms which is bonded to dangling hydrogen atoms at (and very close to) the surface layer. Meanwhile, the O1s photoelectron comes from all the oxygen atoms located near the surface, thus the observed peak in the photoelectron spectrum is a convolution of many peaks which correspond to several surface and bulk species.

It was reported that the O1s binding energy of ice (bulk) observed in the XPS spectrum was shifted by -7.1 eV (without a correction of the work function) or -2.3 eV (with a correction of the work function) compared to H_2O in the gas phase. The O1s binding energy of O1s the less coordinated molecules with the dangling hydrogen at the surface is expected to be between the bulk and the gas phase, because the effect which changes the binding energy in the bulk should be weaker in less coordinated molecules. The present study have shown that the binding energy of such H_2O is shifted by +0.7 eV from the bulk ice, which is thus quite reasonable. This component is not observed in the photoelectron spectrum, this is probably due to the fact that such water molecules with the dangling hydrogen are minor species at the surface of amorphous ice after heated at 60-120K.

In order to verify the above results, we have made a measurements on the H_2O-chemisorbed Si(100) surface at room temperature. The H^+ yield and photoelectron intensities made peaks at similar kinetic energies in the EICO and photoelectron spectra of H_2O/Si(100). This agreement is quite reasonable because all the oxygen on the Si(100) surface is present as OH species bonded to the Si atom as a result of the dissociation of the H_2O molecules at the surface. There is no reason to expect the surface core-level shift of O1s on H_2O/Si(100). This result confirms that the observed difference between the H^+ yield in PEPICO and the photoelectron intensity is due to the core level shift of the H_2O molecules from which hydrogen ion desorbes.

To our knowledge, this is the first observation of the core-level shift on the ice. It demonstrates the advantages and the possibilities of the electron ion coincidence spectroscopy for surface analysis. The EICO spectroscopy can be utilized for an extremely surface sensitive and cite-specific XPS. Moreover, the EICO spectroscopy will be useful to investigate the surface chemical condition because the ion desorption process is strongly related to the surface chemical bond and the relaxation process of the excited state.

(BL2B1)

ORIENTATION OF OXYGEN AD-MOLECULES ON STEPPED PLATINUM (112)

Sugio WAKO,[a] Manami SANO,[a] Yuichi OHNO,[b] Tatsuo MATSUSHIMA,[b] Shin-ichiro TANAKA[c] and Masao KAMADA[d]

[a] *Graduate School of Environmental Earth Science, Hokkaido University, Sapporo 060-0810, Japan*
[b] *Catalysis Research Center, Hokkaido University, Sapporo 060-0811, Japan*
[c] *Department of Physics, Nagoya University, Senju, Nagoya 464-0814, Japan*
[d] *Institute for Molecular Science, Myodaiji Okazaki 444-8585, Japan*

Oxygen molecules on platinum surfaces emit hot atoms parallel to the surface plane when these are photolytically or thermally dissociated. The emission can be directed in a one-dimensional way if the ad-molecules are uni-directionally oriented, which is useful for designing surface aligned reactions. Thus, the orientation of oxygen ad-molecules was examined on stepped Pt(112) at 105 K by near-edge X-ray absorption fine-structure (NEXAFS) [1]. The π^* resonance due to O_2 was major when the electric vector, $\boldsymbol{E}$, of the incident X-ray was in a plane perpendicular to the step edge. On the other hand, when $\boldsymbol{E}$ was in the plane parallel to it, the σ^* resonance was major at the normal incidence and was attenuated with increasing incidence angle of the X-ray whereas the π^* resonance was enhanced. It was concluded that most oxygen was oriented along the step edge, although some oxygen molecules were oriented differently.

EXPERIMENTAL

The angle of X-ray incidence (θ) was varied by rotating the sample crystal such that $\boldsymbol{E}$ was oriented in a plane parallel to or perpendicular to the step edge. The sample crystal was kept at around 105 K during the NEXAFS measurements. The spectra were recorded by an Auger electron yield mode with the kinetic energy of the oxygen KLL Auger electrons at 520 eV. The oxygen coverage (Θ_{O2}) was determined by thermal desorption and normalized to the literature value.

RESULTS

On a clean surface, no signal peaks were found in raw NEXAFS spectra in a photon energy range from 525 eV to 550 eV (Fig. 1a). The difference between this signal and that observed with oxygen yielded NEXAFS due to oxygen ad-molecules (Fig. 1b). The π^* and σ^* resonance states were clearly seen at 530 ± 1 and 535 ± 1 eV. The base line was drawn by considering the edge jump and the energy resolution of the instrument of 2 eV. The energy of the continuum level was considered to begin at 531 eV. The resonance intensity curve was deconvoluted into two Gaussians with a fixed peak position and constant half width.

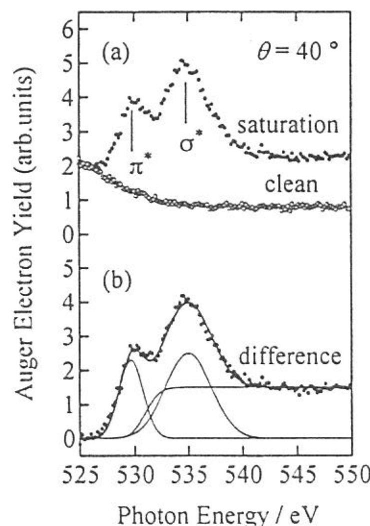

Fig. 1 NEXAFS spectra of oxygen ad-molecules at saturation. $\boldsymbol{E}$ was oriented 40 degrees from the surface in a plane along the step edge. (a) Raw NEXAFS spectra for clean and O_2-saturated surfaces and (b) their difference spectrum. Typical deconvolutions into two Gaussians are shown by the thin curves. The thick solid line indicates the sum of these components.

Both of the resonance peaks showed strong dependence on θ and the crystal azimuth. Furthermore, no coverage dependence was found in NEXAFS spectra over Θ_{O2} = 0.05 to 0.50 (saturation). A series of the spectra at Θ_{O2} = 0.4 is summarized in Fig. 2. The σ * resonance was major at θ =10° when ***E*** was in a plane along the step edge whereas the π * resonance was much less (Fig. 2a). The former decreased quickly with increasing θ and disappeared at around θ =80°, whereas the latter increased with increasing θ. This indicates that oxygen is lying along the step-edge direction. This orientation was supported from NEXAFS when ***E*** was in the plane perpendicular to the step edge (Fig. 2b). The π * resonance was intense irrespective of the incident angle and the σ * resonance was always small. However, it is noteworthy that the latter was always noticeable. Furthermore, the π * resonance was also noticeable at θ =10° when ***E*** was along the step edge. This suggests that some oxygen molecules do not align along the step-edge. When ***E*** was in the plane perpendicular to the step edge, the σ * resonance should disappear when all oxygen molecules align along the step edge. Step edges on stepped platinum surfaces may not be uniform as observed by STM. The molecular axis of oxygen on structural defects may be oriented ±60° from the edge direction because of the terrace with a (111) structure. These oxygen molecules can contribute the σ * resonance even when ***E*** is in the plane perpendicular to the step edge.

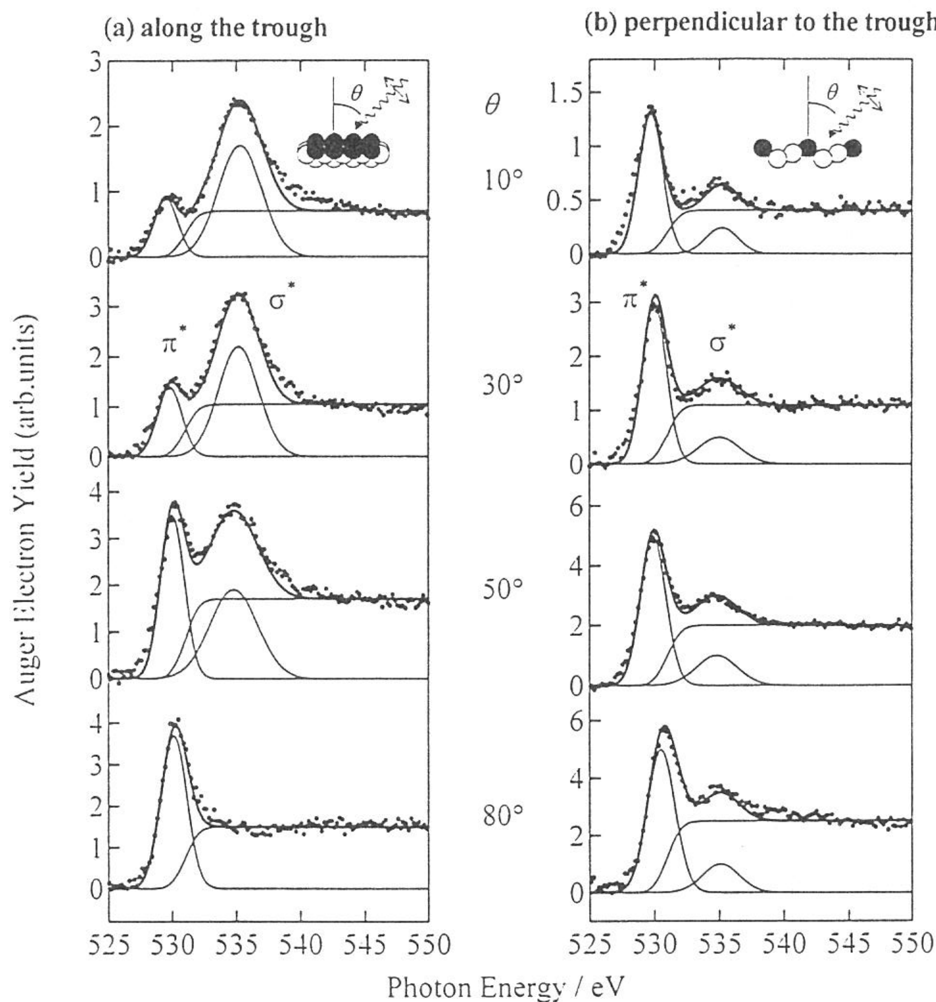

Fig. 2 NEXAFS spectra of oxygen ad-molecules at Θ_{O2}= 0.4 and at various X-ray incident angles. θ is the incidence angle. (a) The electric vector ***E*** was in a plane along the step edge and (b) perpendicular to it. Typical de-convolutions into two Gaussians are also shown.

Reference

[1] M. Sano, Y. Seimiya, Y. Ohno, T. Matsushima, S.I. Tanaka and M. Kamada, Surface Science, **421** (1999) 386.

(BL3A-1)

Deposition of Cu thin films by photo-chemical vapor deposition with Undulator Radiation

H.Sato, M.Uchida, A.Wakahara, A.Yoshida, A.Hoshino* and H.Machida*

Toyohashi University of Technology, Tenpaku, Toyohashi, *441-8580*
*TRI CHEMICAL LABORATORY INC, Japan

Recently, large-scale integrated circuits (LSIs) have been developed remarkably, and mass production in the intrachip connection of 0.25 μ m is advanced. The next step after 0.25 μ m rule, such as 0.15 μ m, are planned on the road map. However, the Al metal as the intrachip circuit wiring material shows the electro-migration, and the resistivity is high. These facts degrade the high speed operation of LSIs. Cu is one of the attractive material, because Cu has an excellent electro-migration tolerance and low resistivity compared with Al. The film growth at low temperature process is possible in the photo-enhanced chemical vapor deposition (photo-CVD), and since low damage and low contamination are expected, it attracts much attention as a process technology in the following generation.

In this study, copper films were deposited on Corning 7059 glass substrates by using photo-chemical vapor deposition with Cu(hfac)(TMVS) (Hexafluoroacetylacetnato Cu(I) · Vinyltrymathylsilane : ($O_2C_5HF_6$)Cu · ($(CH_3)_3Si(CH=CH_2)$)). Undulator Radiation Light was used as the source excitation light source.

The experimental set-up is shown in Fig.1. In this experiment, Corning 7059 glass substrate was installed in the reaction chamber, and Cu(hfac)(TMVS) was supplied by 3×10^{-3} Torr on the substrate. The substrate temperature was always kept below 130 ℃ during the experiments to avoid themal deposition of Cu(hfac)(TMVS). Cu(hfac)(TMVS) is liquid at R.T., and the tube line was heated to 30℃ to avoid condensation of the Cu(hfac)(TMVS). The undulator gap was 60mm, corresponding to the photon energy of 36eV. This photon beam was introduced on the substrate. The average photon density on the surface of the substrate was 7.2 $\times10^{15}$photon/cm^2 · sec, and the total dose was 30000 mA·min.

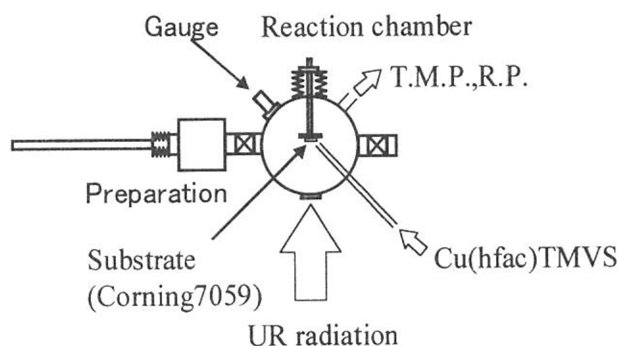

Fig.1. Experimental set-up

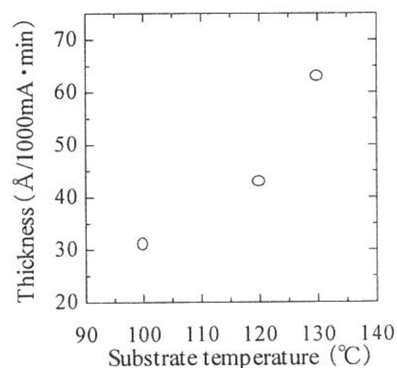

Fig.2. Thickness of the deposited Cu film as a function of the substrate temperature

The relation of the substrate temperature and the film thickness is shown in Fig.2. When the substrate temperature was 130℃, the resistivity of Cu film was very high, but it became 4.7 $\mu\Omega\cdot$cm after annealing (N_2atmosphere, 250℃, 30min, 0.03Torr). When the substrate temperature was 120℃, the resistivity wasn't improved even after annealing.

The surface morphology of the Cu thin-film was observed by atomic force microscope(AFM). The AFM images after annealing are shown in a Fig.3(a), and Fig.3(b). From these images, the grain size was larger with increasing the substrate temperature.

AES spectra after sputter cleaning with Ar ions and annealing are shown in a Fig.5. Carbon was found in the film produced at the substrate temperature of 120℃, but not observed in the film at the substrate temperature of 130℃.

From the above results, it was concluded that the after-annealing is effective in improving the resistivity in the films deposited at higher substrate temperature, resulting in the increase of the grain size and reduction of the impurities in the film.

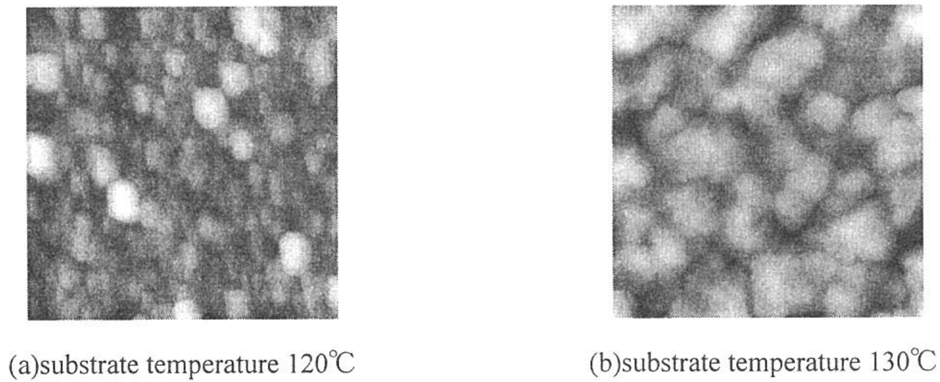

(a)substrate temperature 120℃ (b)substrate temperature 130℃

Fig.3 AFM images of Cu films after annealing (1000nm×1000nm)

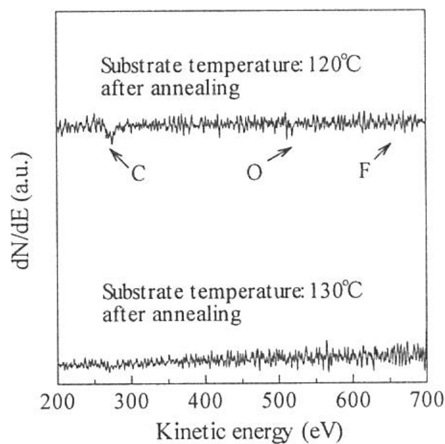

Fig.5. AES spectra after sputter cleaning and annealing.

(BL-4A1)

X-ray photoemission spectroscopy study of Si(111) Surface after Removal of SiO_2 by Synchrotron Radiation Illumination

Yongli Gao[a'], Harutaka Mekaru[a], Tsuneo Urisu[a] and Toshio Horigome[b]

[a]*Institute for Molecular Science, Myodaiji, Okazaki, 444-8585*
[b]*Machine Shop, Japan Advanced Institute of Science and Technology, Tatsunokuchi, Ishikawa, 923-1292*
a' : On sabbatical from Univ. Rochester

X-ray photoemission spectra (XPS) were measured for the native oxide / Si(111) surface after the synchrotron radiation stimulated desorption at the beam line 4A of UVSOR. The optics of the beam line are consisted of one Pt coated elliptically bent cylindrical quartz mirror with 4 degrees grazing incident angle and the horizontal beam divergence of about 15 mrad, and two Pt coated quartz plane mirrors with 2 degrees grazing incident angle. The XPS sample was set about 0.5 m upstream of the focus point. The unmonochromatized XPS apparatus is CL150 from VSW Inc. The resolution of the XPS measurements was about 1.46 eV.

The sample was resistively heated by passing through it a current and the temperature was maintained within ±10 °C as monitored with an optical pyrometer. The structure of the sample holder is shown in Fig. 1. Shown in Fig. 2 are the XPS spectra of Si 2p from oxidized Si(111) surface before and after 8 hours of SR irradiation at beam line 4A. The observed spectrum width is explained by the resolution (about 1.46 eV) of the apparatus. The difference of the spectra is manifested in the part of relative binding energy 2-6 eV. While the spectrum prior to SR irradiation shows the SiO_2 peak at 3.9 eV, the one after SR irradiation has the oxide peak appeared to be centered at 3.6 eV. Previous work by Himpsel et al. shows that SiO_2/Si interface is characterized by intermediate-oxidation states for about two Si layers, twice of that expected for an atomically abrupt interface. The intermediate states, Si^{1+}, Si^{2+}, Si^{3+}, are of relative binding energy 0.95 eV, 1.75 eV, and 2.48 eV, respectively. The observed shift of the oxide peak toward lower relative binding energy therefore reflects the breaking of the bond between Si and O, resulting in the increase of the lesser oxidized Si intermediate states. The benign desorption of the SiO_2 layer by SR stimulated desorption can also contribute to the formation of the steps in registry to the underlying crystal structure and bilayer stripes, since it is less disruptive to the Si surface in comparison to thermal desorption where the consumption of Si to form volatile SiO is taking place.

In Fig. 2, the difference of the intensities of the oxide peaks before and after SR irradiation is quite small in spite of the prolonged SR exposure. One possible factor is the SR photon distribution, since the XPS and STM measurements were performed in two different beam lines, beam lines 4A and 4B, respectively. Not only due to the difference of the calculated total photon flux, the photon flux in beam line 4A is much weaker than beam line 4B in energies larger than 100 eV. For example, at 531 eV (O 2s binding energy), beam line 4A flux is about 6 times weaker than that of beam line 4B. Slower desorption rate observed in XPS result suggests that the core electron excitations of Si (2s : 150 eV and 2p: 108 eV) and O (1s: 531 eV) contribute significantly to the SiO_2 desorption. Another factor may be due to the size of the XPS measurement area, about the 4 mm in diameter, which is larger than the calculated elliptical 7 x 3 mm beam spot and inevitably some areas outside the SR irradiation region were also sampled. Finally, the chamber is turbo-pumped and of base pressure $2x10^{-9}$ Torr, and some contamination of the sample may have occurred.

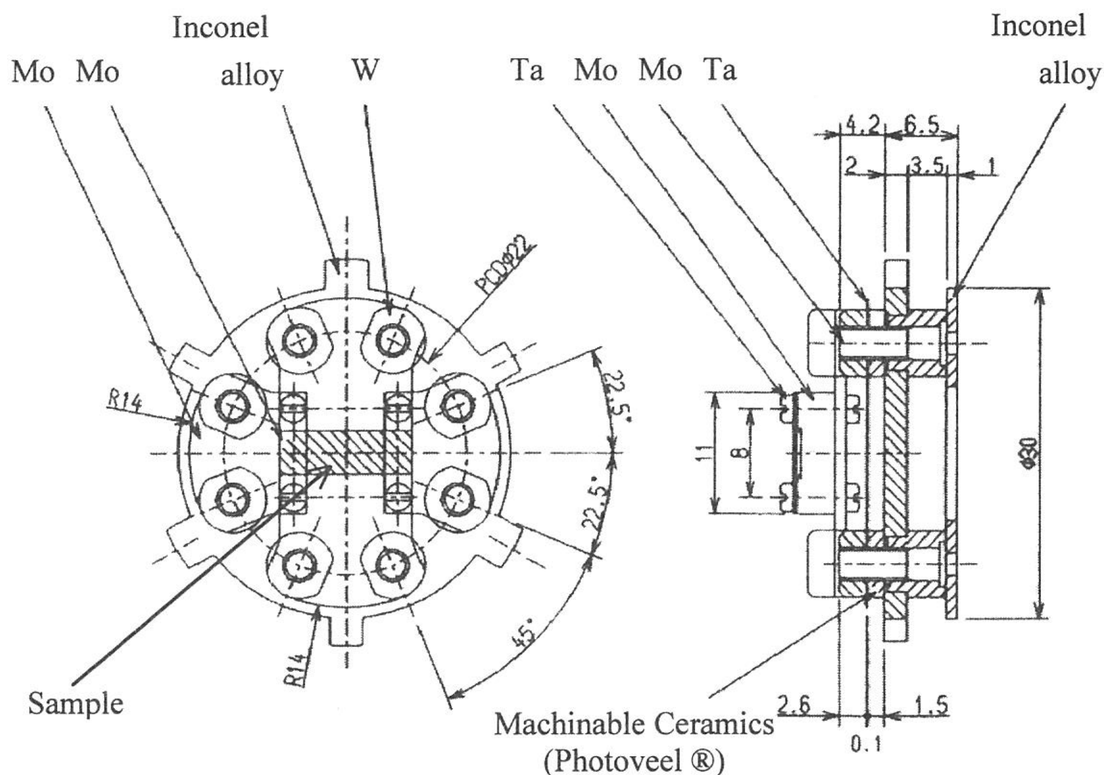

Figure 1. Top and side views of a new type of an XPS sample holder that can be heated at about 1000 K by passing an electric current through the sample.

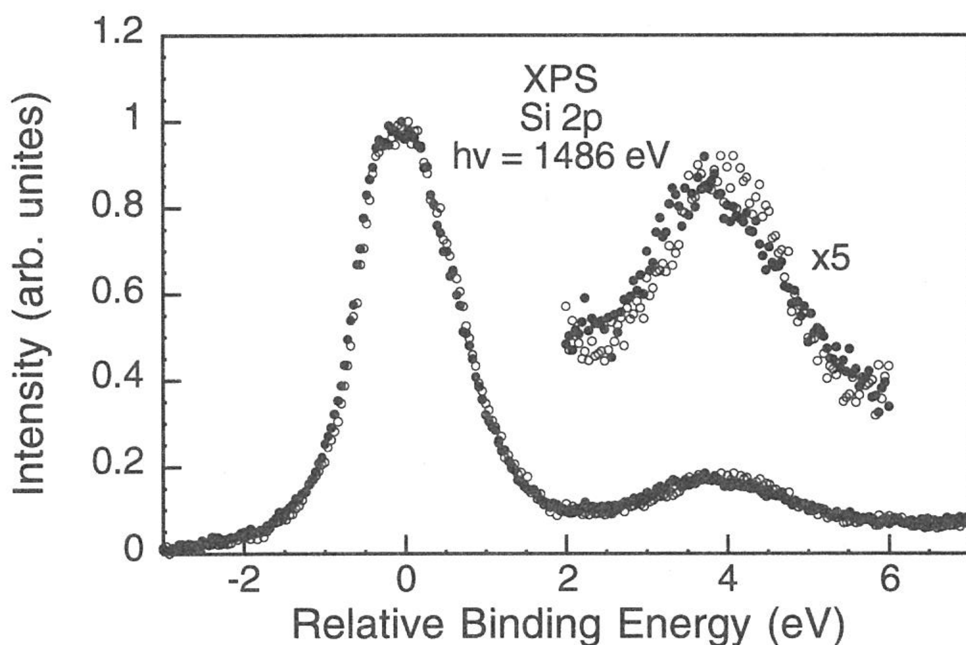

Figure 2. XPS spectra of Si 2p from oxidized Si(111) surface before and after 8 hours of SR irradiation in BL4A. The resolution was 1.46 eV. The difference of the spectra is manifested in the part of relative binding energy 2-6 eV. While the spectrum prior to SR irradiation shows the SiO_2 peak at 3.9 eV, the one after SR irradiation has the oxide peak shifted to 3.6 eV.

(BL-4B)

Scanning Tunneling Microscopy Study of Si(111) Surface Morphology after Removal of SiO_2 by Synchrotron Radiation Illumination

Yongli Gao[a'], Harutaka Mekaru[a] and Tsuneo Urisu[a]

[a]*Institute for Molecular Science, Myodaiji, Okazaki, 444-8585*
a' : On sabbatical from Univ. Rochester

We report the first investigations using scanning tunneling microscopy (STM) on the surface morphology of Si(111) after cleaning (complete removal of surface SiO_2) by SR irradiation. The surface shows large regions of an atomically flat and coherent 7×7 structure. An interesting feature of the surface is the formation of single bilayer steps nicely registered to the underlying crystal structure and the width quantized (to the units of 7×7 unit cell) of stripes formed by the bilayer steps. This indicates that the surface after cleaning reaches thermodynamic equilibrium under SR irradiation at temperatures much lower or by a much shorter time than that necessary for thermal desorption.

The experiment was done at the beam line 4B. The STM measurements were performed with a Rasterscope-3000 from DME Co.. The base pressure of the STM chamber was 5×10^{-10} Torr. Details of the experimental conditions are descrived in Ref. 1. The sample (3×8 mm^2) was an boron doped p type Si(111) wafer of misorientation within ±0.1 degree, with thickness of 0.5 mm and resistivity 8 Ω/cm. A native oxide layer was formed on the Si substrate by a conventional wet process.[1)] The thickness of the native oxide layer was about 1 nm.[2)] The sample was resistively heated by passing through it a current and the temperature was maintained within ±10 °C as monitored with an optical pyrometer. The sample temperature was decreased after cleaning by the rate of 1degree/s down to 700 °C and below this by 2 degrees/s.

The regular shape of the bilayer steps is not associated with the SR stimulated oxide desorption. The topograph of a Si(111) surface prepared by thermal desorption at 880 °C for 2 minutes is shown in Fig. 1(a). No registry of the steps with respect to the underlying crystal structure can be observed. Instead, the steps form arched curves with the ends pinned by particles. In comparison, the Si(111) surface with 2 hour SR irradiation at 700 °C after the oxide layer had been removed by thermal desorption at 880 °C presents the registered steps as shown in Fig. 1(b). This observation indicates that the registered bilayer steps are created through an SR stimulated annealing process. We have also tested 2 hours thermal annealing at 700 °C of Si(111) after thermal desorption of SiO_2 at 880 °C, but could only observe roughened surfaces.

More detailed information about the bilayer steps can be obtained by using finer resolution. Fig. 2 shows the atomic image of a single bilayer step from a Si(111) sample with 2 hours of SR irradiation at 700 °C. The 7×7 structure is clearly visible. The displacement vector g(a,b) between upper and lower terrace 7×7 structures defined by J.L.Goldberg et.al.[3)] is measured to be g(1 + 1/3, 3+2/3) at this step. This indicate that this step is F1a (according to the definition by H. Tochihara *et. al.* [4)]) descending along $[11\bar{2}]$. The 7×7 reconstruction structure is coherent on all over the surface observed by STM (max. 100 x 100nm), and the width of the bilayer stripes are all quantized to the units of the 7×7 cell width similarly as observed in the terrace width of thermal equilibrium Si(111) surface.[5)] These facts indicate that the SR irradiated surface is in thermal equilibrium equivalent to the 700 ℃-20 hours thermal annealing. In summary, we have shown that the SR illumication of Si(111) under elevated temperatures generates a near perfect 7×7 surface with regular shaped bilayer steps. The shape of the steps intend to be hexagonal. The inequivalence of $[\bar{1}\bar{1}2]$ and $[11\bar{2}]$ steps observed in dry chemical etching is absent in the SR irradiation case. The mechanism of the formation of the regular shaped steps can be attributed to the enhancement of the surface migration of Si atoms under SR irradiation and elevated temperatures, which is considered to be induced by the direct photo-excitation of surface adatoms and/or the inelastic cascade scattering of photoexcited electrons. The results may be particularly relevant to the fabrication of Si nanostructures, as nice bilayer stripes of a few unit cell width can be observed.

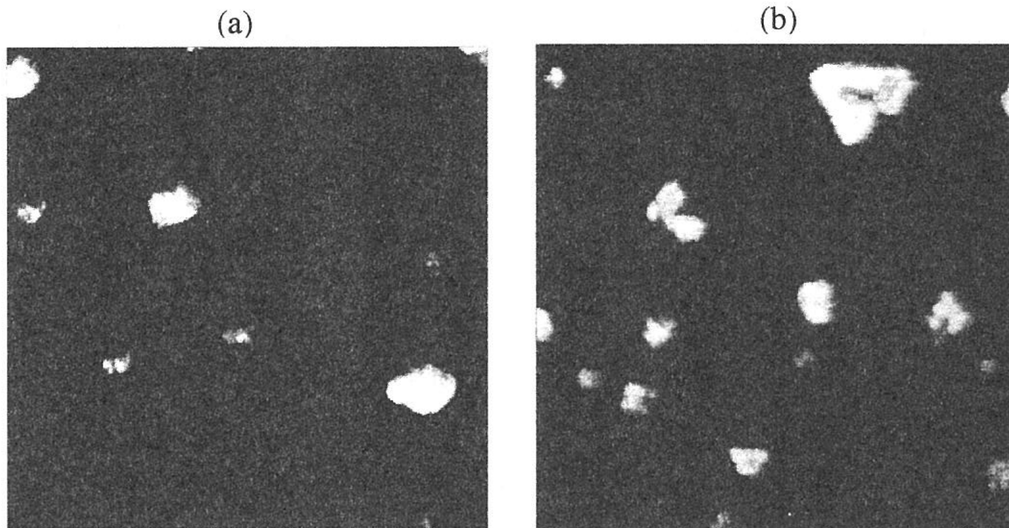

Figure 1. (a) 500 nm×500 nm topograph of a Si(111) surface prepared by thermal desorption at 880 °C for 2 minutes. No registry of the steps with respect to the underlying crystal structure can be observed. Instead, the steps form arched curves with the ends pinned by particles. (b) 200 nm×200 nm topograph of a Si(111) surface with 2 hours SR irradiation at 700 °C after the oxide layer removal by thermal desorption at 880 °C. The registered steps are clearly visible.

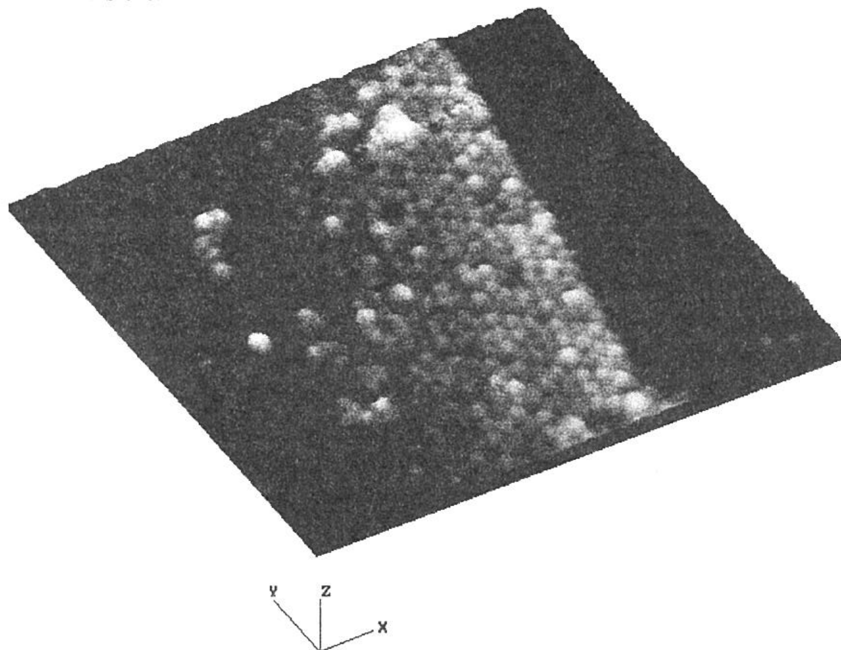

Figure 2. The 3-D atomic image of a bilayer step descending along $[11\bar{2}]$ from a Si(111) sample with 2 hours of SR irradiation at 700 °C.
The 7×7 structure is clearly visible in the 20 nm×20 nm image.

1) T. Miyamae, H. Uchida, I.H. Munro, and T. Urisu, J. Vac. Sci. Technol. A17, 1 (1999).
2) Y. Kobayashi and K. Sugii, J. Vac. Sci. Technol. A10, 2308 (1992).
3) J.L.Goldberg, X.-Swang, J.Wei, N.C.Bartelt, and E.D.Williams, J.Vac.Sci. Technol. A9, 1868 (1991).
4) H.Tochihara, W.Shimada, M.Itoh, H.Tanaka, M.Udagawa, and I.Sumita, Phys. Rev. **B45**, 11332 (1992).
5) X.-S.Wang, J.L.Goldberg, N.C.Bartelt, T.L.Einstein, and E.D. Williams, Phys. Rev. Lett. **65**, 2430 (1990).

BL5A: Formation mechanisms of NEA surface on p-GaAs(100) studied by photoelectron spectroscopy

S. D. More, S. Tanaka), Y. Fujii*) and M. Kamada*

UVSOR Facility, Institute for Molecular Science, Okazaki 444-8585,
**College of Engineering, Osaka City University, Osaka 558-8585*

A dielectric field generated either by an external source or by a heterojunction or a surface dipole can lower the vacuum level of a semiconductor surface below the bulk conduction band level and thus generate a "negative electron affinity" NEA surface.

Negative electron affinity (NEA) surfaces have found applications as efficient photocathodes and the NEA surface of O/Cs/GaAs(100) is known to be a useful emitter of spin-polarized electrons with a high degree of polarization and efficiently. NEA occurs on semiconductors once the vacuum level is pulled below the conduction band minimum.
The photo-induced change in the semiconductor-vacuum interface of a negative electron affinity (NEA) surface prepared by coadsorption of Cs and O on GaAs(100) has been investigated with core level photoelectron spectroscopy using synchrotron radiation and laser light. A mode-locked Ti:Saphire laser with a pulse width of about 160 fs was triggered with a signal from a master oscillator of the UVSOR storage ring. Fundamental light of the laser (photon energy of 1.50 eV) was focused on the sample in a vacuum chamber and spectra have been measured with and without laser irradiation, thus allowing a direct observation of possible band-bending. As substrate a Zn doped ($1x10^{19}$ atoms/cm^3) p-type GaAs(100) wafer was used.

Fig. 1 shows the core level shifts for Ga, As and Cs as a function of sample treatment. The direction of the shifts implies an overall decrease of the band-bending with sample treatment. Superimposed on this trend are corelevel shifts for Ga and As towards lower kinetic energies when Cs is deposited and toward higher kinetic energies when the sample surface is exposed to O. At later stages the direction of the shift is reversed. Cs core level shifts are always towards higher kinetic energies at Cs deposition and lower kinetic energies for O deposition. The amounts of the energy shifts were strongly dependent on the sample treatment [1].

As core level peak shifts do not only indicate band-bending but are also influenced by changes in the chemical environment changes in band-bending have additionally spectra with and without irradition from laser light for clean GaAs, Cs covered GaAs(100) and two surfaces which have been treated with multiple, alternating dosages of Cs and O. They different however in the amount of photocurrent, yielding currents of 0.07 nA and 2 nA.
Both Ga-3d and As-3d photoelectron peaks of the surfaces which have been treated with multiple dosages of Cs and O surface show transient energy shifts of 0.08 eV and less than 0.03 eV, respectively. This compares to values of 0.35 eV for the clean surface and 0.25 eV for the cesium treated sample. This measurement confirms the core-level shift derived observation, indicate that the bands are flattened once the NEA surface condition is approached. It becomes clear however that band flattening itself is not sufficient to achieve NEA surface formation, but might rather be a byproduct of the O interaction at the substrate-Cs interface.

This is contrary to the expectations of previous models and rules out a dipole induced field in the substrate as the origin of NEA surface formation and relocates the workfunction lowering dipole towards a position inside the overlayer.

As Cs-oxide layers exhibit work-functions between 0.6 and 1.5 eV the workfunction of this material is sufficient as a coating to lower the overall work-function of the system. Oxygen-deposition thus first serves to generate Cs-oxide to lower the workfunction, but also interacts with the GaAs substrate. As the height of the interface barrier is critically dependent on the degree of chemical interaction between the substrate and overlayer, oxygen deposition should decrease the interface energy between the overlayer and the substrate.
Conditions for optimal electron yield would therefore be reached when both the workfunction and the interface barrier reach an optimal value.

A synergy of the interface barrier lowering chemical interaction between Cs, O and GaAs, the inherent low electron affinity of Cs-oxides and a possible electron confinement due to surface roughness and micro-domains is proposed to dominate NEA surface formation on GaAs(100) and related surfaces.

A quantitative determination of the interface barrier as a function of oxygen deposition will follow in near future, using the new laser system at BL5A.

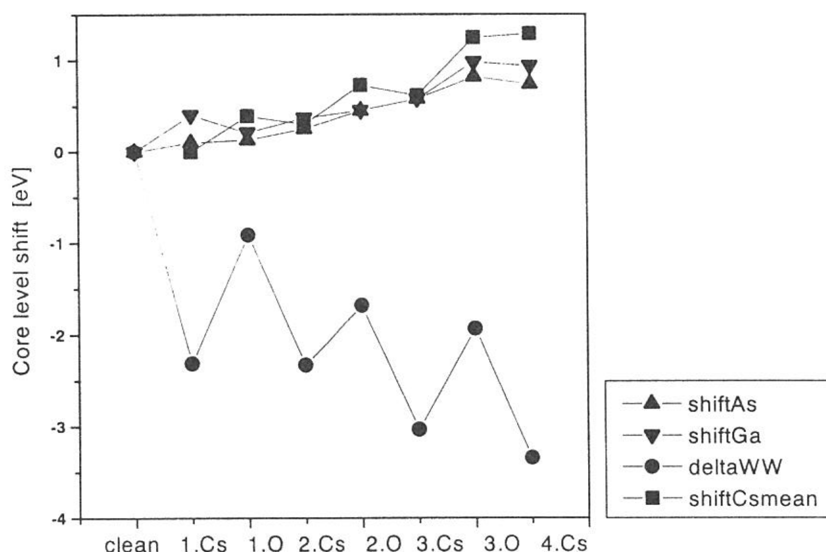

Fig. 1: Core level shifts and workfunction development during NEA surface formation on GaAs(100) [1]

[1] S. More, S. Tanaka, S. Tanaka, Y. Fudjii and M. Kamada, Surf. Sci. in print
[2] N. Takahashi, S. Tanaka, M. Ichikawa, Y.Q. Cai and M. Kamada, J. Phys. Soc. Jap. 66 (1997) 2798

(BL5B)

Absolute Measurements of the Total Yields of Photo-Desorption at the Surface of Solid Argon by Excitonic Excitations

Takashi Adachi*, Satoshi Ishii*, Takato Hirayama*, Ichiro Arakawa*,** and Makoto Sakurai***
*Department of physics, Gakushuin University , Mejiro, Toshima, Tokyo 171-8588.
**Institute for Molecular Science, Myodaiji, Okazaki, Aichi 444-8585.
***Department of Physics, Kobe University, Rokkodai-cho, Nada-ku, Kobe 657-8501.

1. Introduction

Electron or photon irradiation of a solid surface leads the electronic excitations which are followed by the desorption of various kinds of particles. The desorption at the surface of a rare gas solid has been extensively investigated for last two decades[1]. Investigation of this phenomena will reveal dynamics of the electronic excitations and the relaxation processes in the solid. As to the desorption of excited neutral particles from rare gas solids, various desorption mechanisms were proposed and some of them were confirmed experimentally and theoretically. On the other hand, the desorption mechanism of the ground state atom has not been clarified yet, though it is the main component of the desorbed particles. In this report, we present the preliminary results of the absolute measurements of the total photo-desorption yields of argon. The "total" means that we detected all the argon particles desorbed, i.e., atoms and clusters in ground, electronically excited, and ionized states.

2. Experiments

Experiments have been carried out at the beam line BL5B in UVSOR of the Institute for Molecular Science, Okazaki. The wavelength resolution, $\lambda/\Delta\lambda$, was about 500 $\pm$ 200 in the range of λ between 20 and 110 nm. Argon gas was deposited on the surface of a Pt (111) substrate, which is attached to a liquid helium cryostat, at the temperature of 6K or lower. The cryostat was installed in an ultrahigh-vacuum chamber with a base pressure of 5×10^{-9} Pa. The thickness of an argon film was calculated from the exposure on the assumption that the condensation coefficient of the argon on the sample surface was unity. The thickness of argon film was in the range between 1 and 500 atomic monolayers (ML).

Desorption rate was calculated from the rise of the argon partial pressure in the vacuum chamber during the irradiation of the sample. The pumping speed for argon of a turbo molecular pump and the cold surface of the cryostat is 0.09 $\pm$ 0.01 m^3/s in total. The partial pressure of argon was measured by a quadrupole mass spectrometer which was calibrated for argon with an extractor type ionization gauge at each run of the experiments. The absolute intensity of the incident monochromatic vacuum ultraviolet light was monitored by measuring photoelectron current emitted from a gold mesh which was installed in the beam line.

3. Results

The dependence of the absolute photo-desorption yields of argon on the incident wavelength is shown in fig. 1. In case the film thickness is 4 ML film (fig. 1 (a)), a peak is observed at 106 nm which corresponds to the excitation energy for the first order surface exciton (S1). For the film of 100 ML in thickness (fig. 1 (b)), peaks appear at the wavelength corresponding to the second order surface (S2, 96 nm), the first order bulk (B1, 103 nm, 101 nm) and the second order bulk (B2, 91 nm, 90 nm) exciton excitations. The desorption yields which are directly due to excitonic excitations are estimated by the peak height above the continuous background which is thought to be due to the desorption caused by the higher order light from the monochromator. The present systematic measurements of the thickness dependence show that the desorption yields at B1 and B2 excitation increase with the thickness of argon film and reach ~0.07 and ~0.09 Ar/photon, respectively, at 100 ML. The desorption yield at S1 excitation has no thickness dependence and is ~0.03 Ar/photon. On the other hand, the desorption yield at S2 excitation increases gradually with the film thickness and reaches ~0.02 Ar/photon at 50 ML. The origin of the thickness dependence at S2 excitation has not been clarified yet.

(BL5B)

In the case of solid neon[2], the absolute total desorption yields were about 1 and about 2~4 Ne/photon at the bulk exciton excitation and the bulk ionization, respectively. Such large desorption yields of neon were explained by the desorption mechanism which is called "Cavity Ejection (CE)"; the excited atom is pushed out by the repulsive force between the excited atom, which has an expanded electronic orbit, and the surrounding ground state atoms which has negative electron affinity. In the case of neon, the excited atom created at the 2nd or 3rd layer under the surface can desorb via CE mechanism and blow up a number of atoms in over layers because of a small cohesive energy (0.019 eV/atom[3]) in comparison with the kinetic energy of desorbing excited atoms (~0.2 eV[4]). This model, however, can not be applicable in the case of argon because the cohesive energy (0.08 eV/atom[3]) is larger than the kinetic energy of the desorbing excited atom via CE mechanism (~0.035 eV[5]). Other desorption channel of argon atom are thought to be as follows. The dissociation of an excited dimer produces two energetic atoms. The kinetic energy of the dissociated energetic atom is ~0.4 eV[5], which is enough to blow up a number of atoms in over layers. The quantitative analysis of the absolute desorption yields is now in progress.

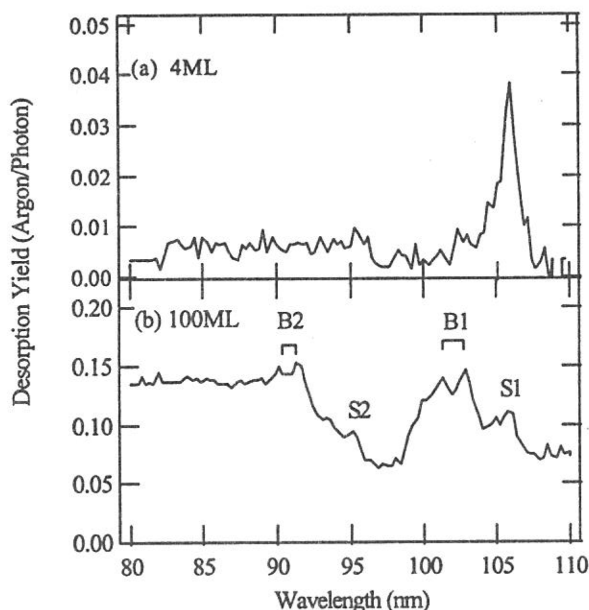

Fig.1 Absolute desorption yields of argon by photon excitation. The thicknesses of argon films are (a) 4 ML and (b) 100 ML.

[1] for recent review, see I. Arakawa, Molec. Crystal Liq. Crystal, **314**, 47 (1998), M. Runne and G. Zimmerer, Nucl. Instrum. Meth. Phys. Res. B **101**, 156 (1995).

[2] I. Arakawa, T. Adachi, T.Hirayama and M.Sakurai, Surf. Sci., accepted for publication.

[3] N. Schwentner, E. -E. Koch and J. Jortner, Electronic Excitations in Condensed Rare Gases, (Springer-Verlag, 1985).

[4] T. Hirayama, A. Hayama, T. Koike, T. Kuninobu, I. Arakawa, K. Mitsuke, M. Sakurai and E. V. Savchenko, Surf. Sci., **390**, 226 (1997).

[5] I. Arakawa and M. Sakurai, in "Desorption Induced by Electronic Transitions IV", eds. G. Betz and P. Varga, (Springer, Berlin, 1990) p. 246.

(BL5A & 6A2)

Time-response of photo-induced core-level shifts in GaAs (100) studied with combination of SR and laser

Masao Kamada, Senku Tanaka[A], Sam Dylan More, Shuji Asaka[B], and Yasuo Fujii[A]

UVSOR Facility, Institute for Molecular Science, Okazaki 444-8585
[A]College of Engineering, Osaka City University, Osaka 558-8585
[B]Equipment Develop Center, Institute for Molecular Science, Okazaki 444-8585

In recent years, we have been studying the non-equilibrium electronic states at semiconductor surfaces using synchrotron radiation and laser. Electric potentials at semiconductor surfaces and interfaces are very important to understand a variety of electrical properties and phenomena of semiconductors and to control semiconductor devices. However, few works have been carried out to understand the dynamics of non-equilibrium charge distribution at the semiconductor surfaces. Long *et al.* have first reported the transient surface photo-voltage on Si (111) using synchrotron radiation (SR) and laser pulses.[1] They obtained non-equilibrium electron density induced by laser pulses in the space charge layer, but the agreement between their experiments and theoretical simulations is not good for a low power laser. In recent years, Marsi *et al.* have reported the time response of the transient surface photo-voltage on Si (111)2x1.[2] The purpose of the present work is to investigate the dynamics of photo-induced carriers on p-GaAs (100), since this surface provides spin-polarized electrons after Cs- and oxygen treatments.

Experiments were carried out at 6A2 and 5A, where a plane-grating monochromator (PGM) and a spherical-grating monochromator (SGM-TRAIN) provide EUV photons, respectively. We used mode-locked Nd:YAG and Ti:Sapphire lasers at BL6A2 and 5A, respectively. Lasers were triggered with a signal from a master oscillator of the UVSOR storage ring. The spatial and temporal overlaps were carefully adjusted by using a MCP-PM/TAC system. The surface of p-type GaAs (100) doped with Zn was prepared *in situ* using usual way.

Figure 1 shows the temperature dependence of the peak shift of Ga-*3d* photoelectron. The observed points can be well fit to the theoretical straight line which was derived on the basis of a thermionic emission model with some approximation. However, this good agreement does not mean that the thermionic emission model is perfect. It is important to obtain temporal information in order to understand the meaning of the carrier density, potential in the surface layer, and so on. Figure 2 shows the temporal structure of the energy shift which was obtained by adjusting the delay time between SR and laser. The observed data can be composed into a fast component in nano-second region and a slow component in the micro- or milli-second region. Hot electrons and holes produced by laser pulses are separately distributed in the surface space-charge layer, and then they will be recombined again to recover the band bending of GaAs. The present result may indicate two pathways at least in the recovering process.

This work was partially supported by a Grant-in-Aid from the Ministry of Education, Science, Culture, and Sports.

Reference: 1) J.P.Long et al., PRL.. 64 (1990) 1158. 2) M. Marsi et al.,APL.. 70 (1997) 895.

Fig. 1. Temperature dependence of the photo-induced energy shift of Ga-3d photoelectron.

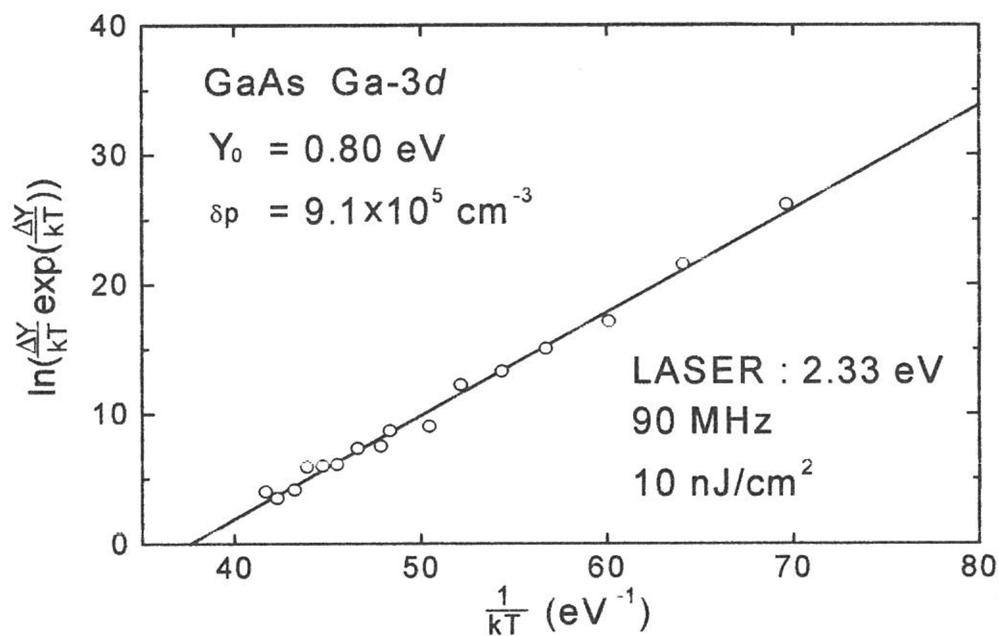

Fig. 2. Temporal structure of the photo-induced energy shift of Ga-3d photoelectron.

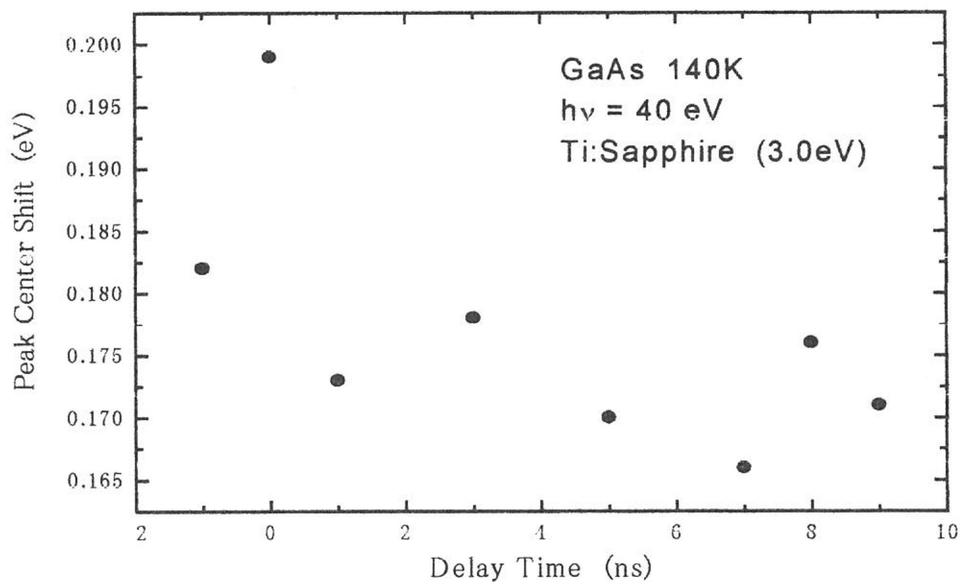

(BL8A)

Ablation of Metal Fluoride Film by Synchrotron Radiation

Hisao NAGAI, Masaru OKUMURA, Seiji ICHIYANAGI, Takumi SHIOMI, Mineo HIRAMATSU, Masahito NAWATA, Masaru HORI* and Toshio GOTO*

Department of Electrical and Electronic Engineering, Meijo University, Tempaku-ku, Nagoya, 468-8502

**Department of Quantum Engineering, Nagoya University, Chikusa-ku, Nagoya, 464-8603*

INTRODUCTION

Fluorine-compound materials including Teflon well absorb photons with energies in vacuum ultraviolet region in synchrotron radiation (SR) beam. Previously, we demonstrated the anisotropic micromachining and film formation of Teflon using the SR ablation process [1,2]. In addition, by selecting the photon energy of SR beam with filter, we indicated that photon energies absorbed by carbon (C) and fluorine (F) atoms contribute to the ablation of Teflon [3]. From results of SR ablation of Teflon, metal fluoride materials consisting of metal and fluorine atoms would be easily etched by the SR irradiation. In this report, the SR ablation process is applied to the etching of metal fluoride films. The anisotropic etching of three types of metal fluoride films, AgFx, MgFx, and AlFx, are systematically demonstrated using the SR ablation.

EXPERIMENT

The experiments were carried out at beam line BL-8A of UVSOR. Three types of metal fluoride films (AgFx, MgFx, AlFx) were prepared on Si substrate by electron beam evaporation. These samples were set perpendicularly to the SR beam in the reaction chamber (base pressure of 10^{-4} Pa). A Nickel (Ni) mesh (square pattern of 77 μm) was used as the contact mask. The SR beam irradiated the samples through the Ni contact mask in vacuum at a room temperature. The etched depth was measured using a surface profiler. The SR-irradiated films were analyzed by scanning electron spectroscopy (SEM) and micro electron spectroscopy for chemical analysis (micro-ESCA).

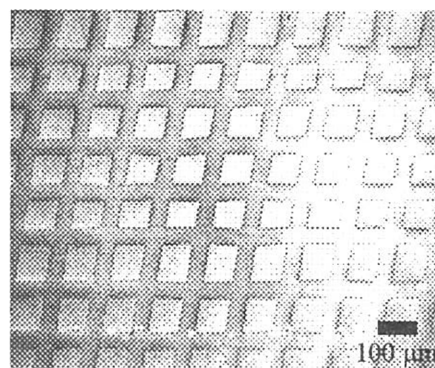

Fig. 1. SEM photograph of fine pattern with 77 μm square holes created in the AlF_x film by SR ablation

RESULTS AND DISCUSSION

Micro-pattern of metal fluoride films (AgFx, MgFx, AlFx) were fabricated by SR ablation process. Figure 1 shows the SEM photograph of fine pattern created in the 50 nm thick AlFx film with the dose of 5000 mA·min. As seen in Fig. 1, the fine pattern of 77 μm square holes was successfully produced in the AlFx film by the SR irradiation. Figure 2 shows the etched depth of AlFx film on Si substrate as a function of SR irradiation time. The thickness of AlFx film prepared on the Si substrate was 50 nm for each sample, and the SR beam current was constant at 190 mA in Fig. 2. When the SR irradiation

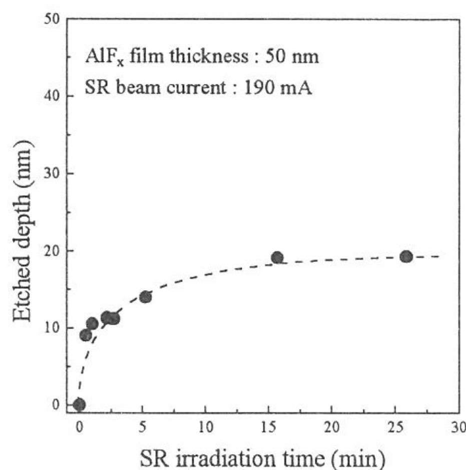

Fig. 2. Etched depth of AlF_x film on Si substrates of a function of SR irradiation time.

time increased, the etched depth of AlFx film increased rapidly at first, then became saturated with further increase of SR irradiation time, resulted in the termination of etching.

Figure 3 shows the F/Al ratios of the SR-irradiated and non-irradiated surfaces of AlFx film on Si substrate measured using micro-ESCA. The change of F/Al ratio corresponds to the created pattern by the SR ablation. Fluorine content of the SR-irradiated area was lower than that of the non-irradiated surface, which suggests that the fluorine atoms would be easy to remove from surface by the SR irradiation compared to the metal atoms.

Figure 4 shows etched depth of AlFx film at which the etching terminated as a function of film thickness of AlFx prepared on Si substrate. In the range of AlFx film thickness investigated, etched depth increased almost linearly with the increase of AlFx film thickness.

Figure 5 shows the etched depth of AlFx film on Au, Ni, SiO_2 and Si substrates as a function of SR irradiation time. The thickness of AlFx film on each substrate was 50 nm, and the SR beam current was constant at 190 mA in Fig. 5. As the SR irradiation time increased, the etched depth increased at first. With further increase of SR irradiation time, however, the etched depth became saturated in all cases. The maximum value of etched depth depended on the substrate materials. In the cases of Au and Ni substrates, Auger electrons ejected from substrates by the SR irradiation would enhance the etching of AlFx film. In the case of SiO_2 substrate, on the other hand, thermal energy due to the absorption of SR in the SiO_2 substrate would enhance the etching of AlFx film.

The SR ablation mechanism including etch termination and effect of substrate materials is under investigation.

SUMMARY

Anisotropic etching of metal fluoride films using the SR-induced reaction was successfully demonstrated. The saturation of etching depended on the thickness of metal fluoride films as well as the substrate materials.

REFERENCES

[1] M. Inayoshi, M. Ito, M. Hori, T. Goto, M. Hiramatsu, and A. Hiraya, Jpn. J. Appl. Phys., 34, L1675 (1995).

[2] M. Inayoshi, M. Ito, M. Hori, T. Goto, and M. Hiramatsu, J. Vac. Sci. Technol., B 17, 949 (1999).

[3] M. Inayoshi, H. Nagai, M. Hori, T. Goto, and M. Hiramatsu, J. Vac. Sci. Technol., submitted.

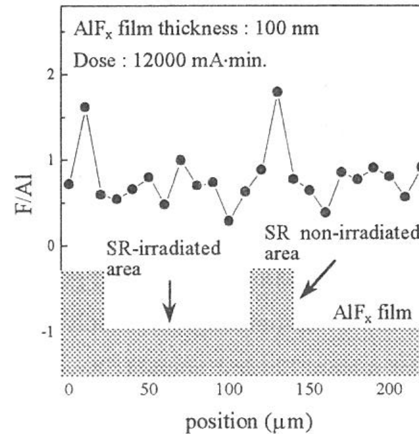

Fig. 3. F/Al ratio of surface of SR irradiated AlF_x film on Si substrate by Micro-ESCA.

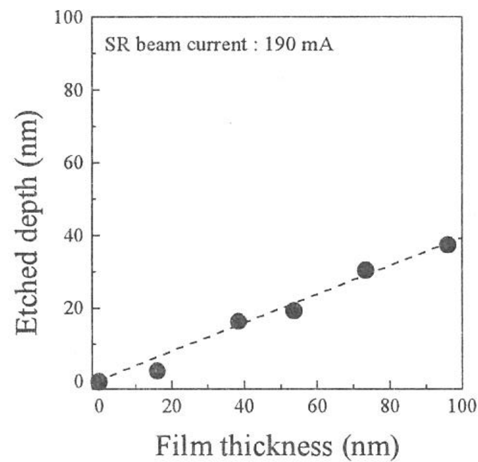

Fig. 4. Etched depth of AlF_x film on Si substrate as a function of prepared film thickness.

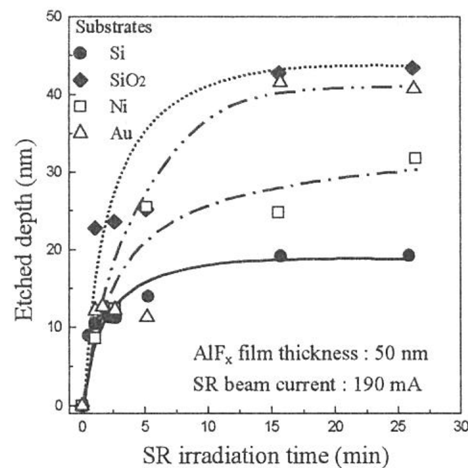

Fig. 5. Etched depth of AlF_x film on Au, Ni, SiO_2 and Si substrates of a function of SR irradiation time.

(BL8A) Growth characteristics and photoluminescence properties of ZnTe homoepitaxial films deposited by synchrotron-radiation-excited growth

Mitsuhiro Nishio, Kazuki Hayashida, Hiroki Harada, Yoshiaki Mitsuishi, Qixin Guo, Hiroshi Ogawa

Department of Electrical and Electronic Engineering, Saga University, Saga 840-8502, Japan

Synchrotron-radiation (SR) excited growth is promising as a new non-thermal technique, since virtually any reactants can be decomposed effectively at low temperature by using a high photon flux density in the vacuum ultraviolet region. Several attempts have so far been carried out using SR light to perform the deposition of semiconductors at low temperatures. In order to improve the film quality, it is important to investigate the photoluminescence (PL) spectrum of the film deposited by SR-excited growth. However, such investigations do not exist except for our previous paper, which described luminescence of ZnTe films deposited under only a confined growth condition. In this study, we describe PL spectra of the ZnTe films deposited under a wide variety of conditions.

The growth experiments were carried out using the SR beam line, BL8A. The beam line supplies only white light. Diethylzinc (DEZn) and diethyltelluride (DETe) were used as source materials. These source materials were independently fed into the chamber together with hydrogen or nitrogen carrier gas by means of mass flow controller and variable leak valve. The deposition of ZnTe was carried out at very low pressure of $10^{-5}\sim10^{-4}$ Torr in the growth chamber.

Figure 1 shows the relationship between the growth rate and DEZn transport rate when DETe transport rate is kept at 1 μ mol/min. The growth rate increases rapidly with increasing DEZn transport rate and then it eventually becomes saturated at low DEZn transport rate around 0.5 μ mol/min. The saturated tendency of the growth rate indicates that the rate-limiting step is due to the supply of DETe. Also, it is suggested that adsorption coefficient of DEZn is very high compared to DETe at room temperature. As shown in the figure, no difference is found in the growth rate between hydrogen and nitrogen carrier gases. Thus, hydrogen seems not to play an important role in the growth reaction due to a use of the low pressure. The PL spectra of ZnTe films as a function of DEZn transport rate are shown in Fig.2 (a), (b), and (c). It is noticeable that the substrate was not heated during growth during growth. The spectra for all samples have a sharply excitonic emission (I_a) at 2.375 eV. The I_a line is attributed to shallow acceptors, namely Li, Cu, and Na. This peak is observed widely for undoped ZnTe grown by another growth methods. The PL spectrum of the film grown at a DEZn transport rate of 1 μ mol/min exhibits the strong deep level emissions with two broad bands centered at around 2.1 eV and 1.85 eV (Fig. 2(a)). The deep-level luminescence may be due to the generation of defects such as vacancy-impurity complex in the film. The deep-level luminescence obtained here can be found in the experimental results by Tews *et al.*, who have attempted laser-induced diffusion in ZnTe with Cl. Thus, a Zn rich condition may facilitate Cl inclusion into a Te lattice site. Actually, a decrease of DEZn transports rate seems to bring about significant reduction of deep level band, as shown in Fig.2 (b), (c). At a DEZn transport rate of 0.5 μ mol/min, only I_a peak can be detected in the spectrum, indicating the relatively good quality film. However, a further decrease in DEZn transport rate leads to two broad bands centered around 2.32 and 2.28 eV in the spectrum of the film, as shown in Fig.2(c). The result for the film obtained at a high transport rate of DETe, which ensures Te rich condition, is given in Fig.2 (d). In the case, the spectrum shows almost the same feature as shown in Fig.2(c). A Te rich condition may occur the contamination of shallow acceptor and/or donor impurities related to these emission

bands. Thus, it seems that the quality of ZnTe film becomes deteriorated under Zn rich and Te rich conditions. Figure 3 shows the PL spectra of ZnTe films as a function of substrate temperature. The PL spectrum depends upon the substrate temperature. The film grown at 60℃ exhibits a strong I_a peak. Two broad bands centered around 2.32 and 2.28 eV are not detected in the spectrum, whereas these are clearly observed in the spectrum of the film deposited at 27℃. However, a further increase in substrate temperature induces enhancement of the deep-level luminescence, as shown in the figure. The spectrum of the film deposited at 100℃ resembles that obtained under a Te rich condition. We have already reported that the growth rate gradually decreases with increasing substrate temperature up to 60℃ and then shows a rapid decrease above this substrate temperature. This behavior will be closely related to the decrease in the adsorbed molecules regarding metalorganic sources with increasing substrate temperature. The PL properties of the films as a function of substrate temperature may be explained with the difference in the temperature dependency of adsorption coefficient between DEZn and DETe molecules.

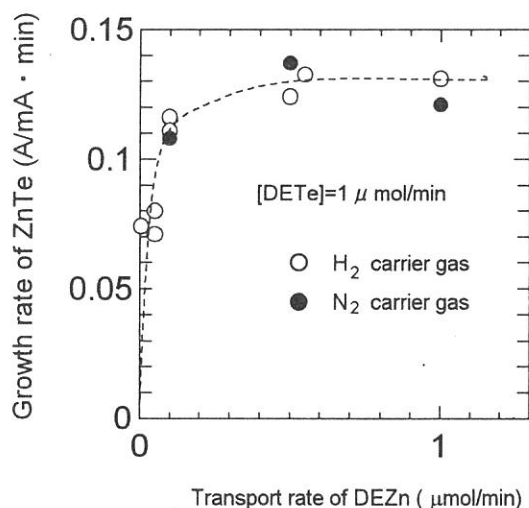

Fig.1. The relationship between the growth rate and DEZn transport rate when DETe transport rate is kept at 1 μ mol/min and substrate temperature at 27℃.

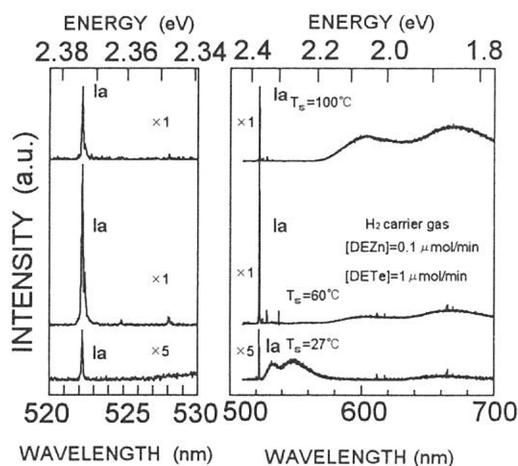

Fig.3. PL spectra of ZnTe films for different substrate temperatures.

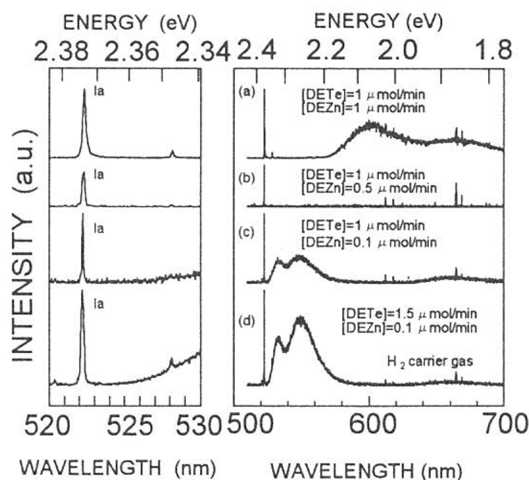

Fig.2. PL spectra of ZnTe films for different DEZn and DETe transport rates when substrate temperature was kept at 27℃.

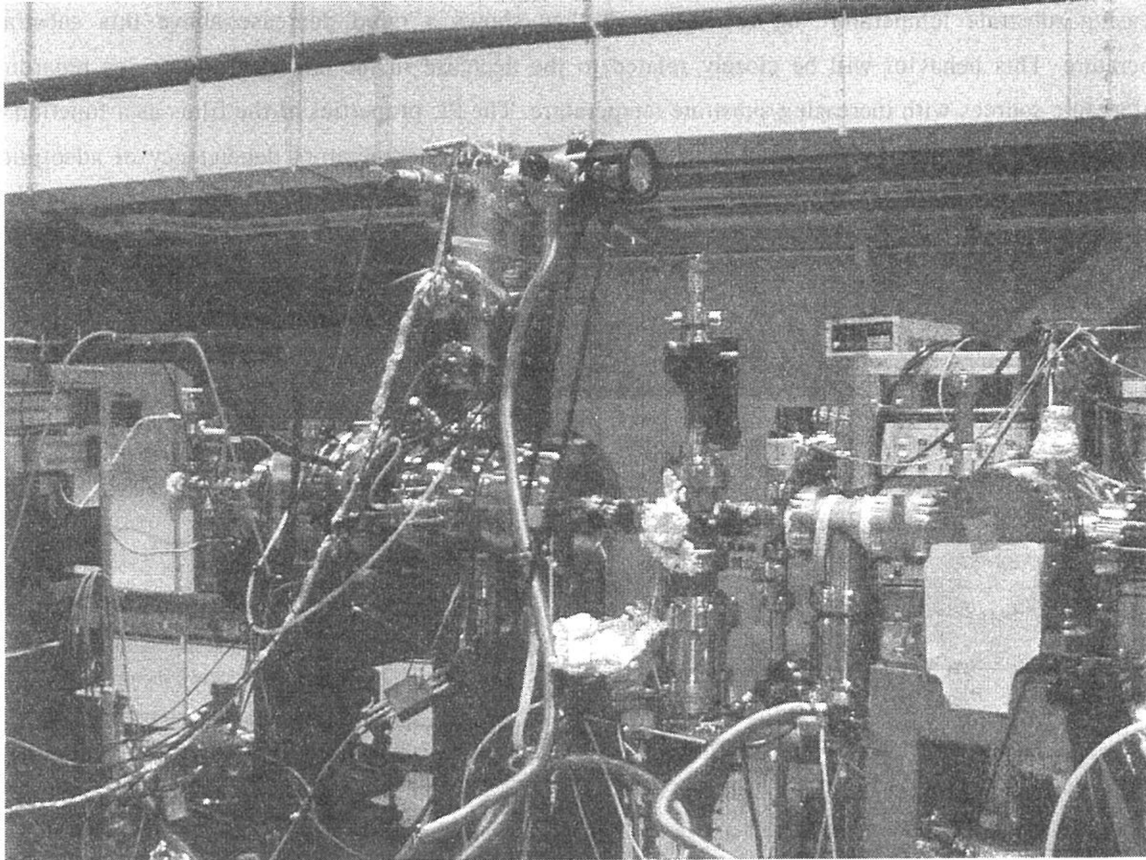

VARTMAN at BL8B1